Turkish Journal of Chemistry

http://journals.tubitak.gov.tr/chem/

Research Article

Turk J Chem
(2018) 42: 958 – 973
© TÜBİTAK
doi:10.3906/kim-1707-77

One-step potentiostatic codeposition and electrochemical studies of poly(1-pyrenyl)-2,5-di(2-thienyl)pyrrole-co-pyrrole) film for electrochemical supercapacitors

Hakan GÖRÇAY[1], **İlhami ÇELİK**[1,*], **Yücel ŞAHİN**[2]

[1]Department of Chemistry, Faculty of Science, Anadolu University, Eskişehir, Turkey

[2]Department of Chemistry, Faculty of Arts and Sciences, Yıldız Technical University, İstanbul, Turkey

Received: 28.07.2017 • **Accepted/Published Online:** 28.01.2018 • **Final Version:** 03.08.2018

Abstract: In this paper, we report a simple, low-cost, and environmentally friendly electrochemical method to obtain a novel copolymer consisting of 1-pyrenyl-2,5-di(2-thienyl)pyrrole and pyrrole on a pencil graphite electrode (PGE). Poly(1-pyrenyl)-2,5-di(2-thienyl)pyrrole-co-pyrrole) that is P(PyrPy-co-Py) film was prepared by one-step potentiostatic codeposition in an ethanol solution containing PyrPy and Py monomers for supercapacitor applications. The electrodeposition of homopolymer and copolymer modified electrodes was carried out on the surface of the PGE via chronocoulometry. For comparison, P(Py)/PGE and P(PyrPy)/PGE were also electrochemically synthesized under the same reaction conditions. The surface morphologies of all the electrode materials were analyzed by field emission scanning electron microscopy. The capacitive properties of the modified PGEs were investigated in 1 M H_2SO_4 electrolyte solution by cyclic voltammetry, electrochemical impedance spectroscopy, and galvanostatic charge-discharge methods. Compared with P(Py)/PGE and P(PyrPy)/PGE, the P(PyrPy-co-Py)/PGE composite exhibited the best electrochemical behavior and had the highest specific capacitance value of 397.18 F g^{-1} in 1 M H_2SO_4 at a scan rate of 2 mV s^{-1}. These results indicated that this modified electrode can be used as an electrode material for electrochemical supercapacitors.

Key words: Supercapacitor, pyrrole, copolymer, electrochemical deposition, electrochemical impedance spectroscopy

1. Introduction

Energy and energy storage are among the most important issues to achieve a clean and sustainable world. In this respect, electrochemical energy storage devices such as batteries, fuel cells, and electrochemical supercapacitors have been recognized as the most important of the various energy storage technologies.[1−5]

Electrochemical capacitors, also called supercapacitors or ultracapacitors, are promising energy storage devices due to their high power density, ultrafast charging-discharging rate, long cycle-life, low cost, excellent stability, and environmental friendliness.[6−10] Among electrochemical energy storage devices, supercapacitors have higher energy density than conventional capacitors as well as higher power density and longer cycle stability when compared with secondary batteries.[11,12] According to their charge storage mechanisms, supercapacitors can be classified into two main categories: electrical double-layer capacitors (EDLCs) and pseudocapacitors.[13−15]

Electrodes that are used in EDLCs usually consist of highly porous materials such as activated carbons, carbon nanotubes, or graphene with very high specific surface areas. In these types of supercapacitors, the charge storage occurs at the interface between electrode and electrolyte. The mechanism of charge storage capacity in

*Correspondence: ilcelik@anadolu.edu.tr

pseudocapacitors depends on the fast faradaic redox reaction between the electrolyte and electrode and transition metal oxides and conducting polymers are used in the electrode materials based on pseudocapacitance.[16–19] Pseudocapacitors can offer far higher specific capacitance and energy density compared to EDLCs due to the presence of the faradaic process.[20,21]

Conductive polymers (CPs) have some advantageous properties including fast doping-dedoping during charge-discharge, high conductivity, easier synthesis, and low cost when compared with metal oxides.[22–24] CPs such as polypyrrole (PPy), polyaniline (PANI), polythiophene (PTh), and their derivatives are promising electrode materials for supercapacitors because of their good electrical conductivity, high capacitance, and low cost.[25–29]

Among them, P(Py) has been widely used for supercapacitor applications because of its high electrical conductivity, high capacitance, and low cost with potential applications for energy storage in wind power systems and electric vehicles.[30–32] On the other hand, P(Py) has some disadvantages, such as its slow kinetics of ion transport due to the poor stability of the redox sites in the polymer backbone during the doping-dedoping process, low cycle-life, and low power density.[33,34] Many studies have been reported including using composites of conductive polymers with carbon materials and preparing their copolymers to solve these problems.[35–41]

Carbon-based substrates have some advantageous properties including a high surface area, low weight, good electrical conductivity, environmental friendliness, and corrosion resistance in aqueous electrolytes, and they could also provide good candidates for templates to support electrochemically active materials for supercapacitor applications. Hereby, these composites improve conductivity, capacitance, power performance, and cycle stability issues that are caused by mechanical problems.[42,43] Among carbon-based substrates, pencil graphite electrodes (PGEs) can be used as electrode material for supercapacitor applications because of having many advantageous properties such as a large active electrode surface area, high electrochemical reactivity, good mechanical rigidity, disposability, low cost, broad electrochemical window, easy modi?cation, and the ability to be miniaturized.[44–46]

An aqueous H_2SO_4 solution can be used as an electrolyte to investigate capacitive properties of electrodes for supercapacitor applications. Supercapacitors generally have low capacitance values because of limited ionic concentration and conductivity in organic electrolytes. At the same time, aqueous-based electrolytes facilitate high power operation because they offer ions of smaller size, higher ionic concentration, and higher mobility compared to nonaqueous electrolytes. In addition, they have some advantages such as low cost and increased safety during operation. In the literature, higher energy density with the use of sulfuric acid electrolytes instead of salt-containing electrolytes confirms that the acid solutions result in higher capacitance and energy density.[47]

The aim of the present investigation was the electrodeposition of P(PyrPy-co-Py) composite film on a PGE to improve the mechanical and electrochemical properties of P(Py) and P(PyrPy) modified electrodes for electrochemical supercapacitor applications. The synthesis of P(PyrPy-co-Py) conductive film and its application has not been reported in the literature. In this respect, 1-pyrenyl-2,5-di(2-thienyl)pyrrole (PyrPy) (Scheme 1) was synthesized by a chemical method. Characterization of PyrPy was carried out by ^{1}H NMR and ^{13}C NMR spectroscopy. P(PyrPy-co-Py) was prepared by one-step electrodeposition on a PGE in this work. The properties of all the modified electrodes were studied in detail using cyclic voltammetry. The capacitive properties of the P(PyrPy-co-Py)/PGE, P(Py)/PGE, and P(PyrPy)/PGE were tested by electrochemical impedance spectroscopy (EIS) and galvanostatic charge-discharge (GCD) methods. The surface morphologies of all modified electrodes were investigated by field emission scanning electron microscopy (FE-SEM).

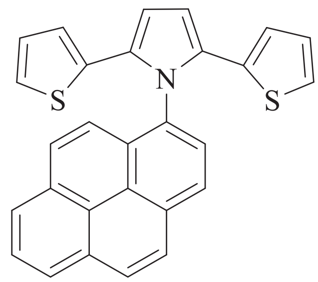

Scheme 1. The molecular structure of 1-pyrenyl-2,5-di(2-thienyl)pyrrole.

2. Results and discussion

2.1. Cyclic voltammetry studies of the monomers

The electrochemical behaviors of PyrPy and Py were studied by cyclic voltammetric method. In addition, a cyclic voltammetry (CV) study involving both monomers was carried out under the same conditions. CV experiments were carried out in nonaqueous solution containing 0.1 M $TBABF_4$ in ethanol (Figure 1). In the experiments, PGE, Ag wire, and Pt wire were used as the working, pseudoreference, and counter electrode, respectively. In the first curve of the cyclic voltammogram, PyrPy exhibited two oxidation peaks at about +0.62 and +0.75 V and a reduction peak at about +0.53 V in ethanol solvent (Figure 1a). Both oxidation and reduction peak current responses increased with increasing number of cycles. The obtained result demonstrates that P(PyrPy) film was formed on the surface of the PGE in ethanol, which was consistent with the published literature.[48] When the electrochemical behavior of Py was examined, the pyrrole monomer was oxidized at about +0.8 V. As shown in Figure 1b, the formation of the broad oxidation and reduction peaks obtained from the cyclic voltammogram indicates the formation of polypyrrole.[49] When CV studies of both monomers are examined, it has been seen that the oxidation and reduction peaks are different from both PyrPy and pyrrole. Moreover, a significant increase in the response of the current density compared with polypyrrole proves the formation of the copolymer (Figure 1c).

2.2. Electrodeposition of P(PyrPy-co-Py) film

The electrocodeposition of P(PyrPy-co-Py) was carried out by chronocoulometry method on the surface of the PGE at a constant potential of +800 mV for 300 s in nonaqueous solution containing 0.001 M PyrPy, 0.05 M Py monomers, and 0.1 M $TBABF_4$ supporting electrolyte in ethanol (Figure 2a). According to Figure 2a, the highest charge density value was obtained and this can prove that P(PyrPy-co-Py) film has better capacitive properties compared with P(Py) and P(PyrPy) films. For comparison, P(Py) and P(PyrPy) modified electrodes were also electrosynthesized under the same reaction conditions (Figures 2b and 2c). All the modified electrodes were cleaned by immersion into ethanol to remove impurities such as electrolytes, monomers, and soluble oligomers remaining on the surface of the electrodes during the polymerization process.

2.3. FE-SEM analysis

The surface morphologies of P(PyrPy), P(Py), and P(PyrPy-co-Py) coated PGE are shown using different magnifications in Figure 3. The surface morphologies of PGEs coated with P(PyrPy) and P(Py) have thin and homogeneous structures (Figures 3a–3f). In contrast, because these modified electrodes do not have more

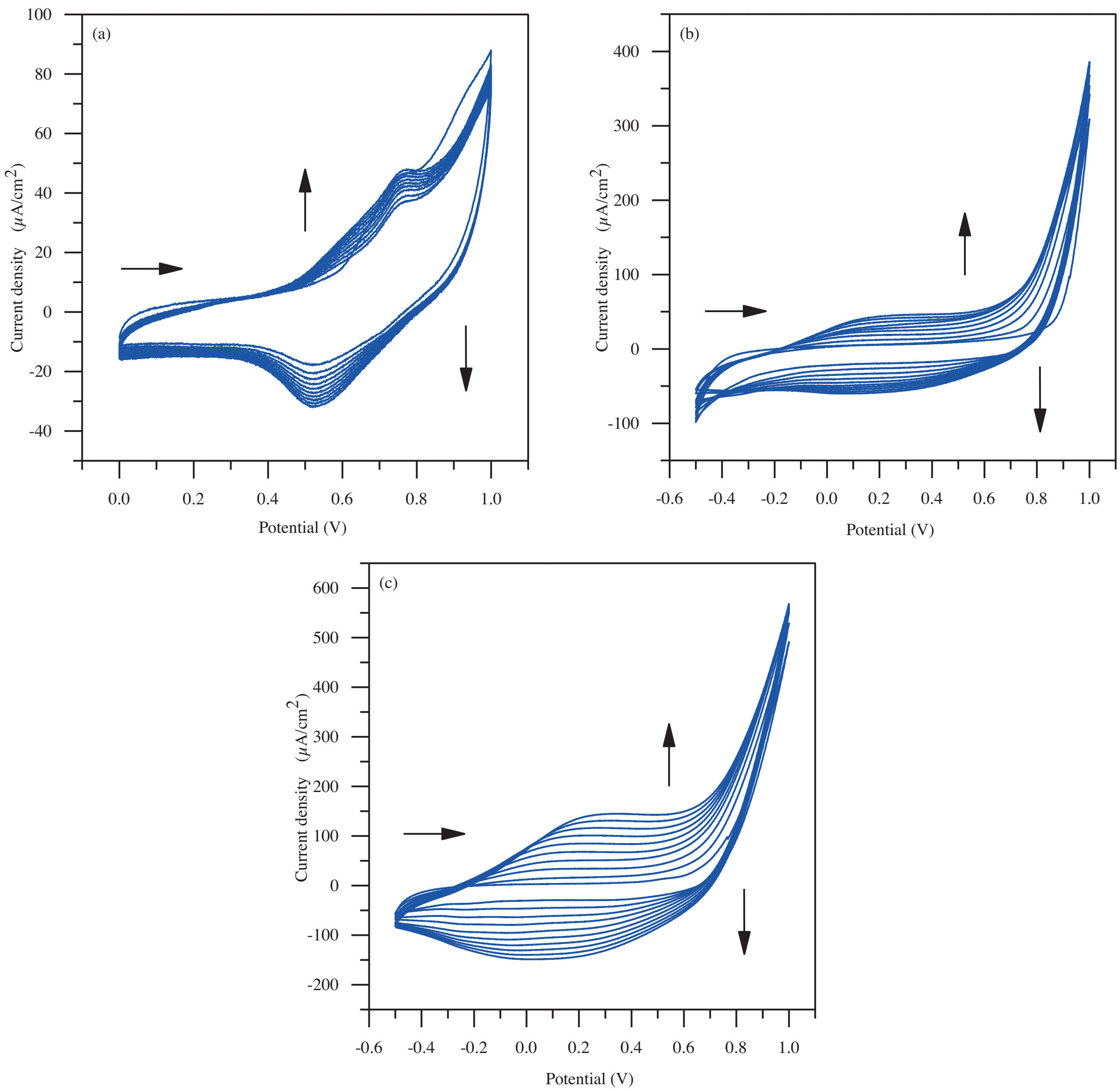

Figure 1. Cyclic voltammograms of (a) PyrPy, (b) Py, and (c) PyrPy-co-Py obtained during polymerization at a scan rate of 100 mV s^{-1} in ethanol (supporting electrolyte: 0.1 M $TBABF_4$; number of scans: 10).

surface area, lower capacitance values were obtained compared to the P(PyrPy-co-Py)/PGE composite. In Figures 3g–3i, the P(PyrPy-co-Py) film has a cauliflower-like nodule structure. The surface of the P(PyrPy-co-Py) modified PGE displayed a more evenly distributed more porous and intense structure (Figures 3g–3i). This is proof that the P(PyrPy-co-Py)/PGE composite has the highest value of capacitance due to having higher surface area.

2.4. Electrochemical behavior of the modified electrodes

In order to evaluate the electrochemical behavior of modified electrodes, CV experiments were performed in 1 M H_2SO_4 electrolyte solution with a three-electrode system. Figure 4a shows a comparison of the cyclic

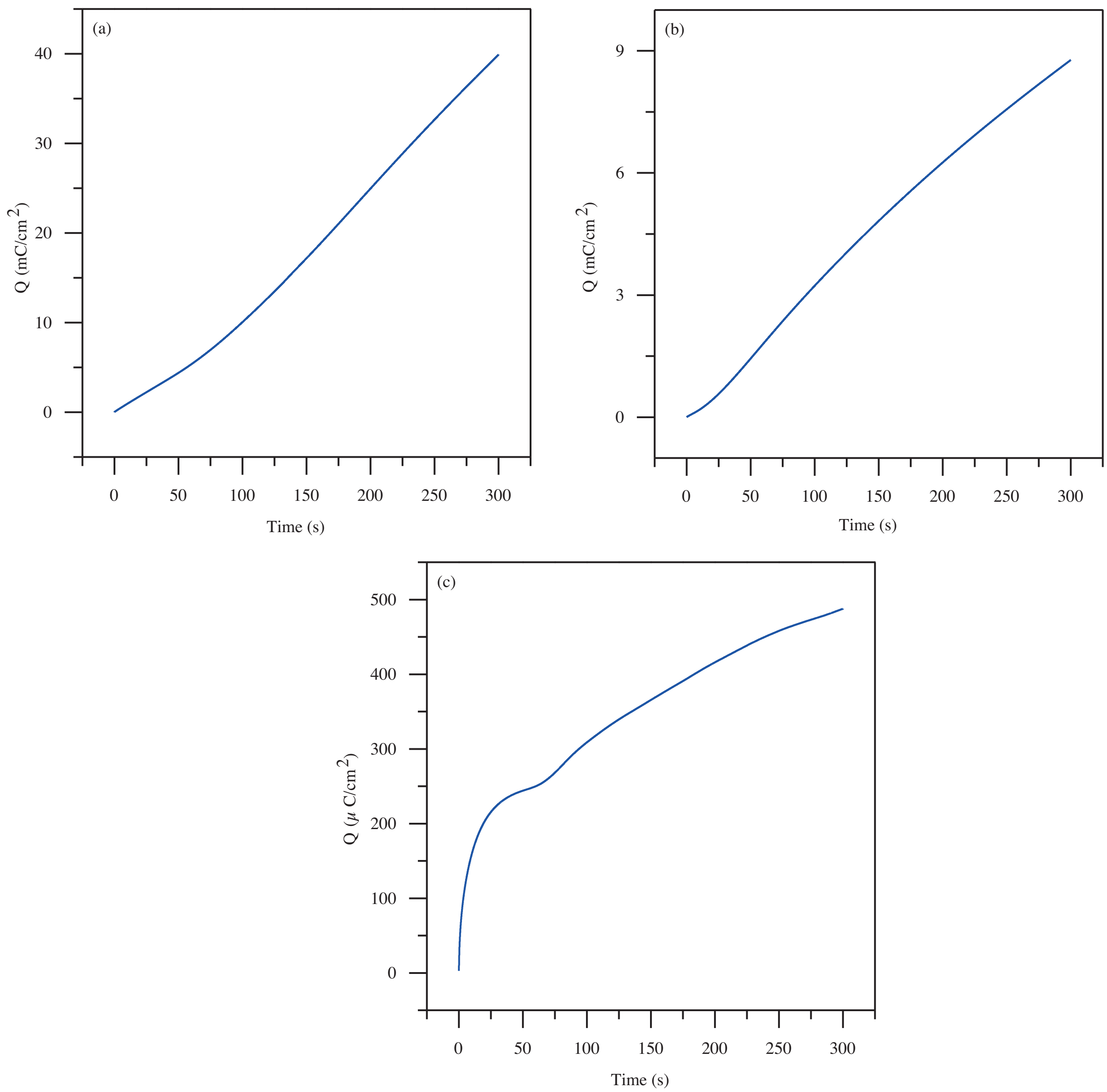

Figure 2. The chronocoulomograms of (a) 0.001 M PyrPy and 0.05 M Py, (b) 0.05 M Py, and (c) 0.001 M PyrPy in 0.1 M $TBABF_4$/EtOH (applied potential: +800 mV; time: 300 s).

voltammograms of P(PyrPy-co-Py)/PGE, P(Py)/PGE, and P(PyrPy)/PGE in the potential range between –0.3 and +0.3 V at a scan rate of 100 mV s^{-1}. In the absence of nonfaradaic processes, the cyclic voltammogram of a supercapacitor should be rectangular in shape, which indicates typical EDLC behavior.[50,51] By contrast, pseudocapacitors (a type of supercapacitor different than EDLCs) are associated with fast faradaic processes that involve reversible redox reactions or faradic charge transfer between the electrolyte and the electroactive species on the electrode surface, and their CV voltammograms deviate from the ideal rectangular shape.[52−54] As can be seen in Figure 4a, the P(PyrPy-co-Py)/PGE and P(Py)/PGE curves exhibited a shape very close to rectangular without any redox peaks, suggesting the good capacitive ability of the modified PGEs. The P(PyrPy-co-

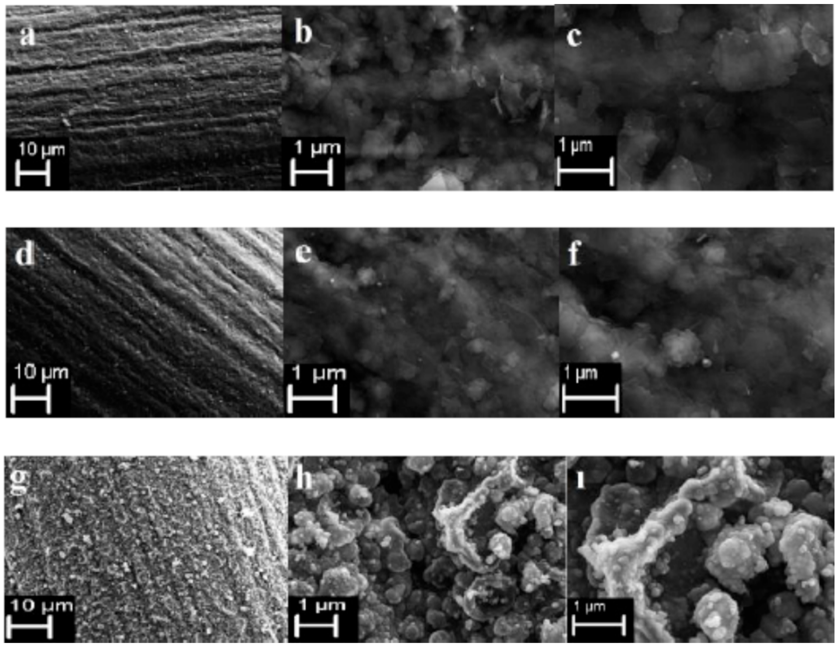

Figure 3. FE-SEM images of P(PyrPy) (a, b, and c), P(Py) (d, e, and f), and P(PyrPy-co-Py) (g, h, and i) modified PGEs.

Py)/PGE composite has larger current response than P(Py)/PGE and P(PyrPy)/PGE, demonstrating a much higher specific capacitance.

Figures 4b–4e show the CV curves of P(PyrPy-co-Py)/PGE, P(Py)/PGE, P(PyrPy)/PGE, and bare PGE at different scan rates from 2 to 100 mV s^{-1} in H_2SO_4 electrolyte solution, respectively. The stable working potential range was determined to be –0.3 to +0.3 V because P(PyrPy-co-Py)/PGE and P(Py)/PGE exhibit a very close rectangular shape in this range. The current responses increased with increasing scan rates for all modified electrodes. Furthermore, a linear relationship between flow responses and different screening rates was observed for all modified electrodes, demonstrating that the faradic processes are diffusion-controlled.[54] This finding is consistent with the results obtained from the EIS analyses. In addition, P(PyrPy-co-Py)/PGE and P(Py)/PGE exhibit a nearly rectangular shape at all scan rates, indicating their good capacitive behavior. In contrast, a significantly distortion from rectangular shape and smaller areas of curves of P(Pyr)/PGE and bare PGE indicate their inferior capacitive performance.[55]

The specific capacitance values of all the modified and bare PG electrodes can be calculated from the CV curves using Eq. (), reported elsewhere:

$$Cs = (1/(m\nu\Delta V)) \int IdV, \tag{1}$$

where C_s (F g^{-1}) represents the specific capacitance, m (g) is the mass of the active material in the electrodes, $\int IdV$ (AV) is the total integrated area of charge and discharge curve of the CV curve, v (V s^{-1}) is the potential scan rate, and ΔV (V) is the potential window of the CV curve.[56,57] From CV experiments, the specific capacitance values of P(PyrPy-co-Py)/PGE, P(Py)/PGE, P(PyrPy)/PGE, and bare PGE were calculated as 397.18, 100.93, 15.75, and 0.000741 F g^{-1} at a scan rate of 2 mV s^{-1}, respectively (Figure 4f). In addition, at the high scan rate of 100 mV s^{-1} these values were obtained as 171.88, 67.82, 1.43, and 0.000236 F g^{-1},

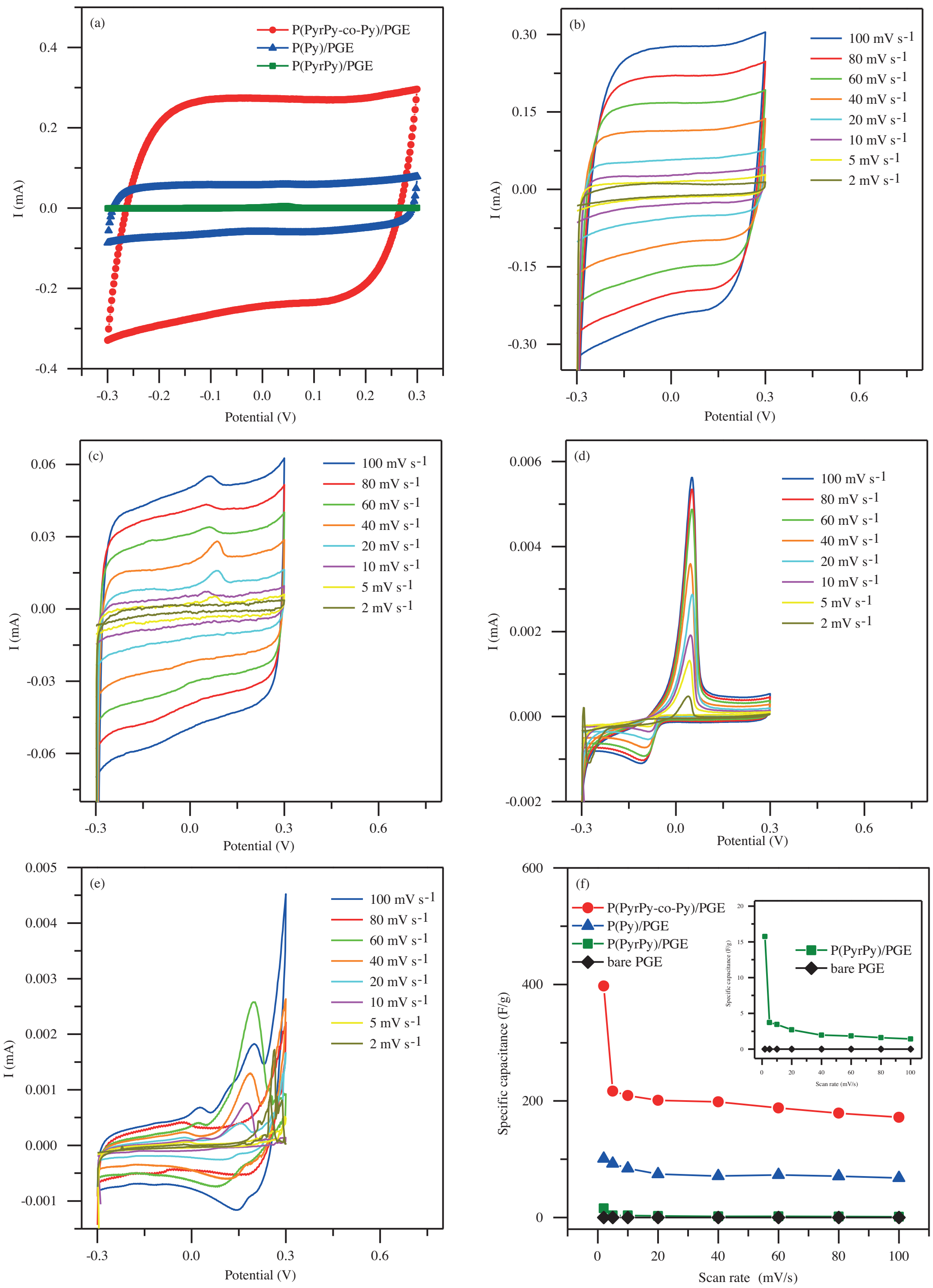

Figure 4. (a) Cyclic voltammograms of P(PyrPy-co-Py)/PGE (●), P(Py)/PGE (▲), and P(PyrPy)/PGE (■) in 1 M H_2SO_4 at a scan rate of 100 mV s^{-1}; (b) CV curves of P(PyrPy-co-Py)/PGE; (c) CV curves of P(Py)/PGE; (d) CV curves of P(PyrPy)/PGE; (e) CV curves of bare PGE at different scan rates ranging from 2 to 100 mV s^{-1} in H_2SO_4; (f) specific capacitance values of all electrodes as a function of scan rate from 2 to 100 mV s^{-1}.

respectively. The highest specific capacitance value achieved at all scan rates for P(PyrPy-co-Py)/PGE is due to the many advantages of P(PyrPy-co-Py) film, such as porous structure, higher surface area, and higher conductivity. As shown in Figure 4f, the specific capacitance values of all electrodes gradually reduced as the scan rates increased from 2 to 100 mV s^{-1}. The presence of internal active sites that cannot complete faradaic transitions at higher scan rates causes such a decrease in capacitance. There are probably incomplete faradaic transitions due to the diffusion effect of the ions in the electrode. The diminishing capacitance indicates that parts of the electrode surface are not accessible at high scan rates.[58] These capacitance values are different from the values obtained by EIS and GCD measurements for all electrodes. It can be considered that cyclic voltammetry, EIS, and GCD methods will not provide similar results depending on the different parameters measured in each case.[47] As a result, the best results were obtained for the PGE with modified P(PyrPy-co-Py) film compared to P(Py)/PGE, P(PyrPy)/PGE, and bare PGE.

The capacitive property or the charge storage mechanism of the conducting polymers or copolymers can be explained by their faradaic properties that are related to the anion and cation insertion/extraction processes. A^- denotes the anions of the electrolyte in the reaction. The SO_4^{2-} ions situated in the supporting electrolyte easily diffuse into and out of the copolymer chain during faradaic processes in order to neutralize the immobilized charge of the P(PyrPy-co-Py) film by the insertion of anions. The anodic and cathodic faradaic processes indicate the release and incorporation of sulfate ions to the copolymer chain.[59] The faradaic reaction can be demonstrated as in Scheme 2.

$$\mathbf{P(PyrPy\text{-}co\text{-}Py) + A^-} \underset{\textbf{Discharging}}{\overset{\textbf{Charging}}{\rightleftharpoons}} \mathbf{P(PyrPy\text{-}co\text{-}Py)^+ A^- + e^-}$$

Scheme 2. Faradaic reaction of P(PyrPy-co-Py) film.

2.5. Electrochemical impedance spectroscopy measurements

The electrochemical behaviors of all electrodes at the electrode–electrolyte interface were investigated by EIS (Figure 5). Figure 5a displays the Nyquist spectra of P(PyrPy-co-Py), P(Py), and P(PyrPy) composite PG electrodes recorded in 1 M H_2SO_4 under potential amplitude of 10 mV and frequency of 0.01 Hz to 100 kHz. In the high frequency region, the intercept of the Nyquist curve on the real axis gives the solution resistance (R_s), which is the resistance in contact with the electrode and the electrolyte.[60] The presence of the semicircle indicates charge transfer resistance (R_{ct}) at the electrode–electrolyte interface that is obtained from diameter of the semicircle in the high frequency region.[61] At the low frequency region the 45° slope of the straight line of the Nyquist plots is the Warburg resistance (W), which results from diffusion of ions in the electrolyte.[62] According to the EIS spectra, semicircles were observed at the high frequency region for P(PyrPy-co-Py) and P(Py) composite electrodes. The R_{ct} values were about 2 Ω for these electrodes, which suggests that the interfacial charge-transfer resistances were quite low. This was also attributed to fast ion and electron transfer in the electrodes. It is obvious that bare PGE exhibited a much larger R_{ct} than other electrodes due to low conductivity, which hinders its electrochemical properties (Figure 5b)[63]. The slope of P(PyrPy-co-Py)/PGE was larger than that of the P(Py) and P(PyrPy) composite electrodes in the low frequency region. This result indicates the low diffusion resistance of the electrolyte ions in the electrode structure, which shows the high specific surface area of the copolymer supports better capacitive behavior of P(PyrPy-co-Py) compared to P(Py) and P(PyrPy) modified electrodes.

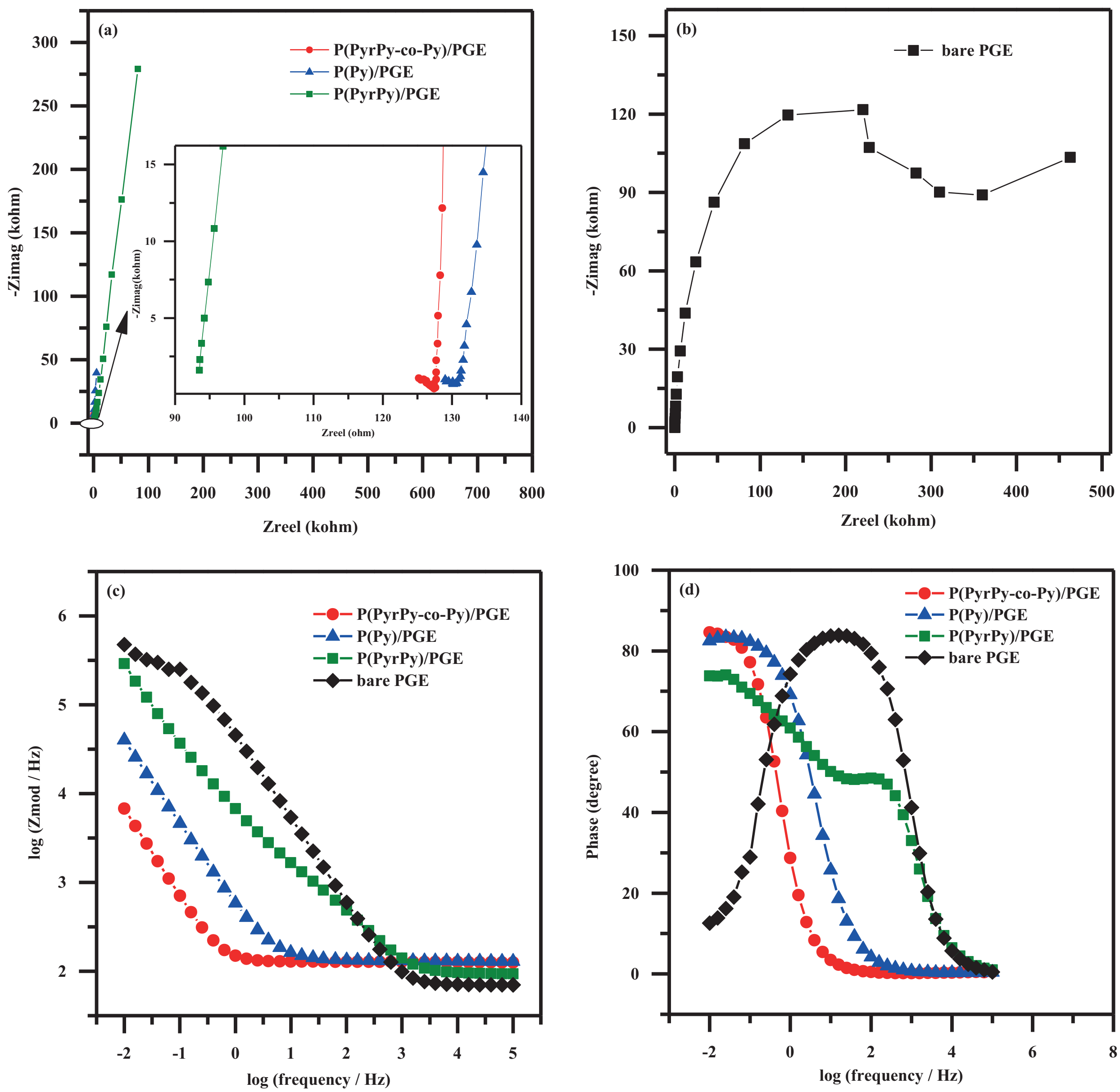

Figure 5. The Nyquist spectra of (a) P(PyrPy-co-Py)/PGE (●), P(Py)/PGE (■), and P(PyrPy)/PGE (▲); (b) bare PGE (♦); (c) Bode magnitude plots versus log frequency of all electrodes; (d) Bode plots of phase angle versus log frequency of all electrodes in 1 M H_2SO_4.

The low frequency capacitance (C) values of all modified PGEs and bare PGE (at 0.01 Hz) were calculated from the imaginary component (Z_{im}) of the impedance at low frequencies by using the following equation:

$$C = (2\pi f Z_{im})^{-1}, \tag{2}$$

where C is the capacitance, Z_{im} is the imaginary component of impedance, and f denotes the frequency.[64] The specific capacitance values of P(PyrPy-co-Py)/PGE, P(Py)/PGE, and P(PyrPy)/PGE composites were calculated as 109.46 F g^{-1}, 35.82 F g^{-1}, 10.19 F g^{-1}, and 0.0029 F g^{-1}, respectively. According to the obtained results from EIS analyses, P(PyrPy-co-Py)/PGE exhibits the highest specific capacitance value when compared to (PyrPy)/PGE, P(Py)/PGE, and bare PGE.

The magnitude of the impedance (Z) versus the log frequency values is shown in Figure 5c. The lowest impedance value was obtained for P(PyrPy-co-Py)/PGE, which is due to its better capacitive property. Figure 5d represents the Bode phase angle plot, which is important for explaining the quality of the active electrode material. An ideal capacitor indicates an exact –90° phase angle at low frequencies.[65,66] In general, phase angles approaching –90° confirm better capacitive properties and fast charge-discharge processes. From Figure 5d, the phase angle values are found to be –84.60°, –82.47°, –73.82°, and –12.59° in the low frequency region for P(PyrPy-co-Py)/PGE, P(Py)/PGE, (PyrPy)/PGE, and bare PGE, respectively. The obtained results indicate that P(PyrPy-co-Py)/PGE has the best capacitive property compared to the (PyrPy)/PGE, P(Py)/PGE, and bare PGE.

2.6. Galvanostatic charge-discharge experiments

Galvanostatic charge-discharge tests of the prepared composite electrodes were carried out in a potential range of –0.3 to +0.3 V with a three-electrode system at a current density of 2 A g^{-1}. Figure 6 shows the galvanostatic discharge curves of P(PThPy-co-Py)/PGE, P(Py)/PGE, and P(PyrPy)/PGE in 1 M H_2SO_4 at a current density of 2 A g^{-1}. The capacitance values of the modified PGEs can be calculated by the obtained galvanostatic discharge curves in Figure 6 according to Eq. (3):

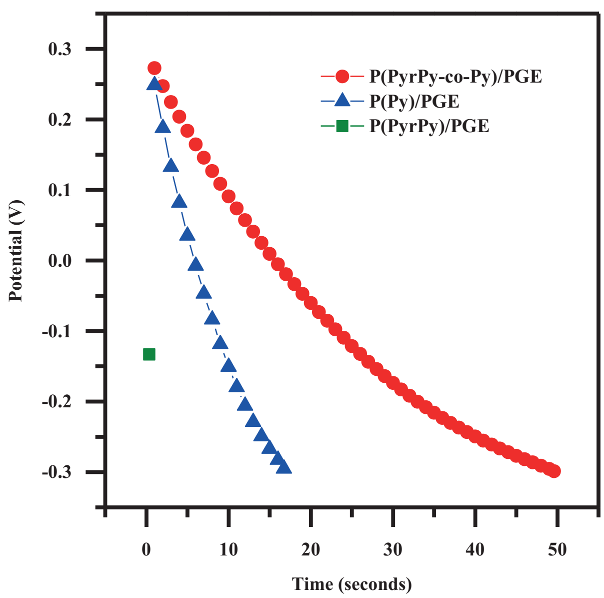

Figure 6. Galvanostatic discharge curves of P(PThPy-co-Py)/PGE (●), P(Py)/PGE (■), and P(PyrPy)/PGE (▲) in 1 M H_2SO_4 at a current density of 2 A g^{-1}.

$$C = I\Delta t/\Delta V, \tag{3}$$

where C (F) is the capacitance of the electrode, I is the constant discharge current (A), Δt (s) is the discharge time, and ΔV (V) is the potential window.[67] The specific capacitance, C_m (F g^{-1}), is obtained by dividing the capacitance by the mass of the difference of the PGE before and after electrodeposition.

According to the above equation, the specific capacitance values of P(PyrPy-co-Py)/PGE, P(Py)/PGE, and P(PyrPy)/PGE were found to be 178 F g^{-1}, 65 F g^{-1}, and 0.8 F g^{-1} at 2 A g^{-1} constant current density, respectively (Figure 7a). Compared with P(Py)/PGE and P(PyrPy)/PGE, the highest specific capacitance obtained at the P(PyrPy-co-Py)/PGE composite can be attributed to the high conductivity of P(PyrPy-co-Py) film, the fast insertion/extraction of doping ions in P(PyrPy-co-Py)/PGE, and the high effective surface area of the P(PyrPy-co-Py) composite PGE.

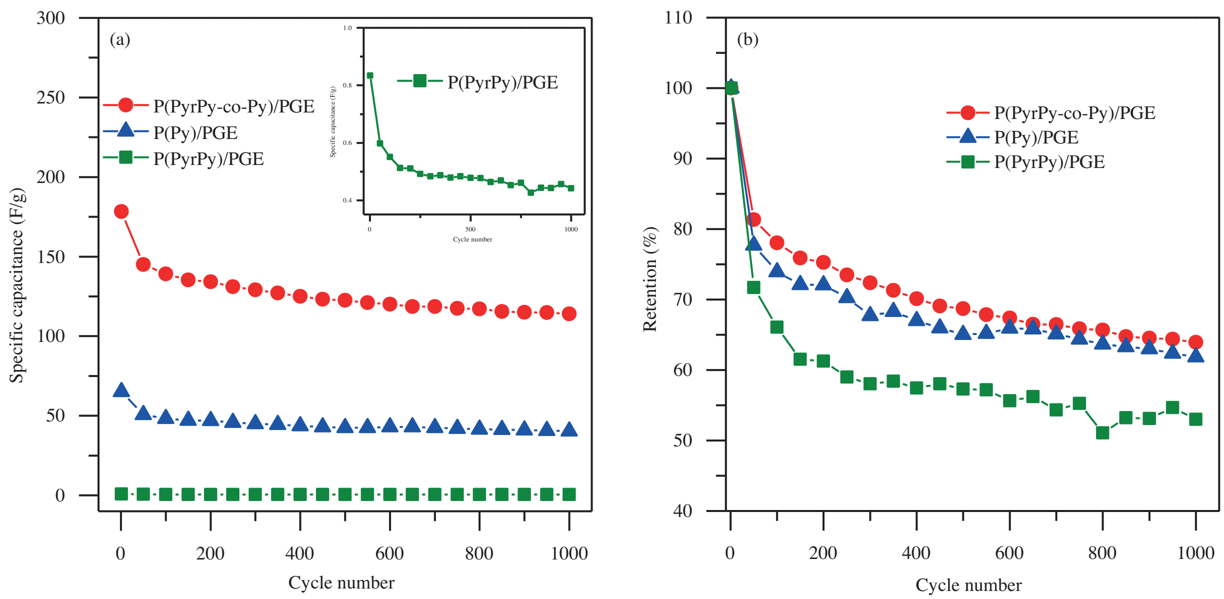

Figure 7. (a) Specific capacitance values (specific capacitance of P(PyrPy)/PGE (■) is also shown as inset) and (b) capacitance retention of P(PyrPy-co-Py)/PGE (●), P(Py)/PGE (▲), and P(PyrPy)/PGE (■) in 1 M H_2SO_4 at a constant current density of 2 A g^{-1} for 1000 cycles.

In the literature, various electrode materials have been reported for supercapacitor applications. Among these studies, polypyrrole (PPy), polyphenylpyrrole (PPhPy), and polymethoxyphenylpyrrole (P(MPhPy)) were synthesized electrochemically onto carbon fiber microelectrodes by Sarac et al.[68] The specific capacitance values for these electrodes were calculated as 0.44 F g^{-1}, 0.038 F g^{-1}, and 0.046 F g^{-1}, respectively. Ates et al. reported a PPy/CuO nanocomposite synthesized by electrochemical method onto a glassy carbon electrode and found a specific capacitance value of 20.78 F g^{-1} at 5 mV s^{-1} scan rate in H_2SO_4 electrolyte solution.[69] In another work, a fiber-shaped carbon nanotube polypyrrole electrode was electrochemically prepared and the specific capacitance value of this electrode was obtained as 56 F g^{-1} in polyvinyl alcohol/H_2SO_4 gel electrolyte including hydroquinone at 0.2 A g^{-1} constant charge-discharge current density.[70] Biswas and Drzal developed a nanoarchitecture of a graphene nanosheets and polypyrrole nanowires composite electrode, which exhibits 165 F g^{-1} specific capacitance at 1 A g^{-1} discharge current density.[71] Wolfart et al. electrosynthesized an imidazole modified poly(pyrrole) copolymer onto stainless steel and reported the specific capacitance reached 201 F g^{-1} at 10 mV s^{-1} in 1 M H_2SO_4 electrolyte solution.[72] It is concluded that the specific capacitance value obtained for P(PyrPy-co-Py)/PGE is satisfactory compared to those of other similar structures from the literature.

Figure 7b displays the capacitance retention of P(PyrPy-co-Py)/PGE, P(Py)/PGE, and P(PyrPy)/PGE in 1 M H_2SO_4 at a constant current density of 2 A g^{-1}. As shown in Figure 7b, the capacitance retentions of P(Py)/PGE and P(PyrPy)/PGE were reserved by 62% and 53% after 1000 charging-discharging cycles, respectively. However, the P(PyrPy-co-Py)/PGE composite has a higher capacitance retention value at 64% after 1000 cycles. These results demonstrate that the copolymer modified PGE has enhanced cycling stability.

2.7. Conclusions

A facile and inexpensive method has been reported to produce a new P(PyrPy-co-Py) conductive film consisting of the direct electrosynthesis of 1-pyrenyl-2,5-di(2-thienyl)pyrrole and pyrrole on a PGE as electrode material for supercapacitors. 1-Pyrenyl-2,5-di(2-thienyl)pyrrole (PyrPy) was synthesized chemically and characterized by ^{1}H NMR and ^{13}C NMR spectroscopic techniques. Electrochemical deposition of a new P(PyrPy-co-Py) thin film was carried out on the PGE by using chronocoulometry and it was used as electrode material for electrochemical supercapacitors for the first time in the present study. The morphological properties of the copolymer and homopolymer modified electrodes were studied by scanning electron microscopy technique. The capacitive behaviors of the modified electrodes were examined by cyclic voltammetry, EIS, and GCD experiments. It has been demonstrated that the P(PyrPy-co-Py)/PGE had an enhanced specific capacitance value compared to pure P(Py) and P(PyrPy) modified electrodes, resulting from its better electrochemical features. Specific capacitance of 397.18 F g^{-1} was achieved for the P(PyrPy-co-Py)/PGE composite, which was almost 4-fold higher than 100.93 F g^{-1} for P(Py)/PGE and 25-fold higher than 15.75 F g^{-1} for P(PyrPy)/PGE composite in 1 M H_2SO_4 at a scan rate of 2 mV s^{-1}. Because the P(PyrPy-co-Py)/PGE composite has better electrochemical performance than pure P(Py)/PGE and P(PyrPy)/PGE, it can be proposed as an electrode material for electrochemical energy storage devices.

3. Experimental

3.1. Materials and chemicals

Thiophene (Fluka, ≥98%), succinyl chloride (Sigma-Aldrich, 95%), dichloromethane (HPLC grade, 99.9%), aluminum chloride ($AlCl_3$, Fluka, 98%), sodium bicarbonate ($NaHCO_3$, Fluka, ≥99.9%), magnesium sulfate ($MgSO_4$, Across, 97%), 1-aminopyrene (Sigma-Aldrich, 95%), paratoluene sulfonic acid (*p*-TSA, Fluka, 99%), toluene (Carlo Erba, 99%), sulfuric acid (H_2SO_4, Sigma-Aldrich, 98%), tetrabutylammonium tetrafluoroborate ($TBABF_4$, Sigma-Aldrich, 99%), and ethanol (Sigma-Aldrich, ≥99.8%) were of analytical grade and used without further purification. Glassware was routinely oven-dried at 110 °C for a minimum of 4 h. Column chromatography was performed on silica gel, 70-230 mesh. Pyrrole (Fluka, ≥97%) was freshly distilled. Aqueous solutions were prepared by using ultrapure deionized water (Sartorius).

3.2. Equipment

NMR spectra of the monomer were recorded on a DD2 400 MHz spectrometer (^{1}H at 400 MHz and ^{13}C at 100 MHz) in $CDCl_3$ with TMS as the internal standard. Preparation of modified electrodes was performed using a VoltaLab PGZ402 controlled by VoltaMaster 4 software. CV experiments, EIS measurements, and charge-discharge experiments of modified electrodes were carried out using a Gamry Instruments Reference 3000.

The surface morphologies of the prepared electrodes were observed with an ultrahigh resolution field emission scanning electron microscope (Zeiss-Ultraplus) at an accelerating voltage of 15 kV.

3.3. Chemical synthesis of 1-pyrenyl-2,5-di(2-thienyl)pyrrole

1,4-Di(2-thienyl)-1,4-butanedione was synthesized by a previously reported method.[73] A solution of 500 mg (2 mmol) of 1,4-di(2-thienyl)-1,4-butanedione, 434 mg (2 mmol) of 1-aminopyrene, and a catalytic amount of *p*-TSA in dry toluene was refluxed in a Dean-Stark apparatus until all the starting materials disappeared on TLC. The flask was cooled and the solvent was removed under reduced pressure. The residue was placed in a silica gel column with dichloromethane to give the pure PyrPy derivative. The synthetic route of the PyrPy is shown in Scheme 3.

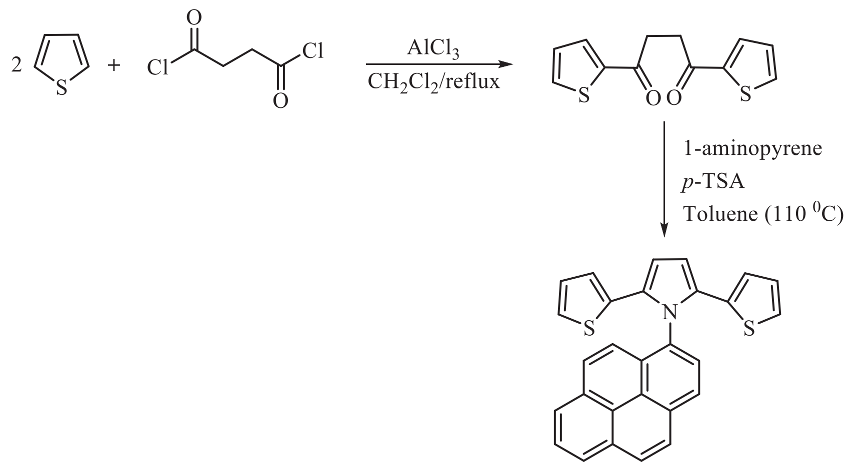

Scheme 3. Synthetic route of 1-pyrenyl-2,5-di(2-thienyl)pyrrole.

Yield: 64%; orange solid; mp = 244–246 °C. ^{1}H NMR (400 MHz, $CDCl_3$): δ(ppm) 8.24 (t, J= 7.8 Hz, 2H), 8.16 (q, J= 7.5 Hz, 3H), 8.04 (d, J= 8.0 Hz, 2H), 7.99 (d, J= 9.2 Hz, 1H), 8.07 (d, J= 9.6 Hz, 1H), 6.78–6.76 (m, 3H), 6.54 (t, J= 4.0, 2H), 6.35 (d, J= 3.6 Hz, 2H). ^{13}C NMR (100 MHz, $CDCl_3$): δ(ppm) 134.7, 132.1, 132.0, 131.4, 131.1, 131.0, 130.1, 129.3, 128.6, 128.0, 127.0, 126.7, 126.5, 125.9, 125.9, 124.9, 124.3, 123.6, 123.6, 122.1, 109.7.

3.4. Preparation of modified electrodes

Electrodeposition of P(PyrPy-co-Py), P(Py), and P(PyrPy) proceeded at the surface of PGEs by chronocoulometry. A conventional three-electrode system was used for all measurements; PGEs were used as the working electrode. A silver wire and a platinum wire were used as the reference electrode and counter electrode, respectively. All electrochemical experiments were carried out under ambient conditions.

A Noki pencil, Model 2000 (Japan), was used as a holder for graphite leads (Tombow, HB, 0.5 mm diameter, Japan). Electrical contact with the lead was obtained by soldering a metallic wire to the metallic part. PGEs were washed with water and ethanol to remove the impurity and dried at room temperature before the experiments. Then the PGE was immersed in the polymerization solution. The modified electrodes were obtained by electrodeposition on the surface of the working electrodes in ethanol solutions of 0.1 M $TBABF_4$. Electrochemical deposition was performed using a VoltaLab PGZ402 controlled by VoltaMaster 4 software.

3.5. Electrochemical impedance spectroscopy

EIS measurements were performed in 1 M H_2SO_4 electrolyte solution at room temperature using a conventional three-electrode cell configuration. In all impedance measurements, modified PGEs, silver wire, and platinum wire were used as working, counter, and reference electrodes, respectively. The electrochemical cell was connected to a potentiostat (Gamry Reference 3000) interfaced to a computer. EIS measurements were recorded in the frequency range from 100 kHz to 10 mHz at open circuit potential with an alternate current amplitude of 10 mV.

3.6. Morphological analysis

The morphological features of the modified electrodes were exhibited with an ultrahigh resolution field emission scanning electron microscope (Zeiss-Ultraplus) at an accelerating voltage of 15 kV. The graphite electrodes were attached on a metal holder by use of double-sided carbon tape. FE-SEM measurements were carried out via the Zeiss-Ultraplus.

Acknowledgment

Financial support from the Anadolu University Research Projects Commission (Project No.: 1401F016) is gratefully acknowledged.

References

1. Yu, A.; Chen, Z.; Maric, R.; Zhang, L.; Zhang, J.; Yan, J. *Appl. Energ.* **2015**, *153*, 1-2.
2. Wei, F.; Jiang, J.; Yu, G.; Sui, Y. *Mater. Lett.* **2015**, *146*, 20-22.
3. Dorraji, M. S. S.; Ahadzadeh, I.; Rasoulifard, M. H. *Int. J. Hydrogen Energ.* **2014**, *39*, 9350-9355.
4. Xu, X.; Shen, J.; Li, N.; Ye, M. *Electrochim. Acta* **2014**, *150*, 23-34.
5. Vidyadharan, B.; Misnon, I. I.; Ismail, J.; Yusoff, M. M.; Jose, R. *J. Alloy. Compd.* **2015**, *633*, 22-30.
6. Chen, Y.; Du, L.; Yang, P.; Sun, P.; Yu, X.; Mai, W. *J. Power Sources* **2015**, *287*, 68-74.
7. Zhou, J.; Huang, Y.; Cao, X.; Ouyang, B.; Sun, W.; Tan, C.; Zhang, Y.; Ma, Q.; Liang, S.; Yan, Q. et al. *Nanoscale* **2015**, *7*, 7035-7039.
8. Shaikh, S. F.; Lim, J. Y.; Joo, O. S. *Curr. Appl. Phys.* **2013**, *13*, 758-761.
9. Li, J.; Xie, H.; Li, Y. *Mater. Lett.* **2014**, *124*, 215-218.
10. Srimuk, P.; Luanwuthi, S.; Krittayavathananon, A.; Sawangphruk, M. *Electrochim. Acta* **2015**, *157*, 69-77.
11. Xie, Y.; Du, H.; Xia, C. *Micropor. Mesopor. Mat.* **2015**, *204*, 163-172.
12. Huang, K. J.; Zhang, J. Z.; Fan, Y. *J. Alloy. Compd.* **2015**, *625*, 158-163.
13. Ng, C. H.; Lim, H. N.; Hayase, S.; Harrison, I.; Pandikumar, A.; Huang, N. M. *J. Power Sources* **2015**, *296*, 169-185.
14. Chen, W.; Xia, C.; Rakhi, R. B.; Alshareef, H. N. *J. Power Sources* **2014**, *267*, 521-526.
15. Miao, F.; Shao, C.; Li, X.; Zhang, Y.; Lu, N.; Wang, K.; Liu, Y. *Int. J. Hydrogen Energ.* **2014**, *39*, 16162-16170.
16. Hsu, C. T.; Hu, C. C.; Wu, T. H.; Chen, J. C.; Rajkumar, M. *Electrochim. Acta* **2014**, *146*, 759-768.
17. Chen, J.; Xia, Z.; Li, H.; Li, Q.; Zhang, Y. *Electrochim. Acta* **2015**, *166*, 174-182.
18. Ye, Y.; Zhang, H.; Chen, Y.; Deng, P.; Huang, Z.; Liu, L.; Qian, Y.; Li, Y.; Li, Q. *J. Alloy. Compd.* **2015**, *639*, 422-427.
19. Teng, S.; Siegel, G.; Prestgard, M. C.; Wang, W.; Tiwari, A. *Electrochim. Acta* **2015**, *161*, 343-350.
20. Xu, J.; Sun, H.; Li, Z.; Lu, S.; Zhang, X.; Jiang, S.; Zhu, Q.; Zakharova, G. S. *Solid State Ionics* **2014**, *262*, 234-237.

21. Yu, L.; Yang, B.; Liu, Q.; Liu, J.; Wang, X.; Song, D.; Wang, J.; Jing, X. *J. Electroanal. Chem.* **2015**, *739*, 156-163.

22. Zhou, H.; Han, G.; Xiao, Y.; Chang, Y.; Zhai, H. J. *Synth. Met.* **2015**, *209*, 405-411.

23. Hashmi, S. A.; Upadhyaya, H. M. *Solid State Ionics* **2002**, *152-153*, 883-889.

24. Xiao, Q.; Zhou, X. *Electrochim. Acta* **2003**, *48*, 575-580.

25. Alvi, F.; Ram, M. K.; Basnayaka, P. A.; Stefanakos, E.; Goswami, Y.; Kumar, A. *Electrochim. Acta* **2011**, *56*, 9406-9412.

26. Chen, W.; Xia, C.; Rakhi, R. B.; Alshareef, H. N. *J. Power Sources* **2014**, *267*, 521-526.

27. Fathi, M.; Saghafi, M.; Mahboubi, F.; Mohajerzadeh, S. *Synth. Met.* **2014**, *198*, 345-356.

28. Xu, J.; Hou, J.; Xiao, Q.; Wei, Q.; Zhang, R.; Zhang, S.; Pu, S. *Mater. Lett.* **2006**, *60*, 1156-1160.

29. D'Eramo, F.; Zon, M. A.; Fernandez, H.; Sereno, L.; Arevalo, A. H. *Electrochim. Acta* **2008**, *53*, 7182-7190.

30. Su, Y.; Zhitomirsky, I. *Appl. Energ.* **2015**, *153*, 48-55.

31. Zhu, Y.; Shi, K.; Zhitomirsky, I. *J. Power Sources* **2014**, *268*, 233-239.

32. Keskinen, J.; Tuurala, S.; Sjödin, M.; Kiri, K.; Nyholm, L.; Flyktman, T.; Strømme, M.; Smolander, M. *Synth. Met.* **2015**, *203*, 192-199.

33. Hu, J.; Wang, H.; Huang, X. *Electrochim. Acta* **2012**, *74*, 98-104.

34. Liang, B.; Qin, Z.; Li, T.; Dou, Z.; Zeng, F.; Cai, Y.; Zhu, M.; Zhou, Z. *Electrochim. Acta* **2015**, *177*, 335-342.

35. Qia, K.; Qiua, Y.; Guo, X. *Electrochim. Acta* **2014**, *137*, 685-692.

36. Alvi, F.; Ram, M. K.; Basnayaka, P. A.; Stefanakos, E.; Goswami, Y.; Kumar, A. *Electrochim. Acta* **2011**, *56*, 9406-9412.

37. Wang, P.; Zheng, Y.; Li, B. *Synth. Met.* **2013**, *166*, 33-39.

38. Shen, K.; Ran, F.; Zhang, X.; Liu, C.; Wang, N.; Niu, X.; Liu, Y.; Zhang, D.; Kong, L.; Kang, L. et al. *Synth. Met.* **2015**, *209*, 369-376.

39. Weng, Y. T.; Tsai, C. B.; Ho, W. H.; Wu, N. L. *Electrochem. Commun.* **2013**, *27*, 172-175.

40. Lai, L.; Wang, L.; Yang, H.; Sahoo, N. G.; Tam, Q. X.; Liu, J.; Poh, C. K.; Lim, S. H.; Shen, Z.; Lin, J. *Nano Energ.* **2012**, *1*, 723-731.

41. Muthulakshmi, B.; Kalpana, D.; Pitchumani, S.; Renganathan, N. G. *J. Power Sources* **2006**, *158*, 1533-1537.

42. He, X.; Gao, B.; Wang, G.; Wei, J.; Zhao, C. *Electrochim. Acta* **2013**, *111*, 210-215.

43. Sarker, A. K.; Hong, J. D. *Colloid Surface A* **2013**, *436*, 967-974.

44. Frackowiak, E.; Beguin, F. *Carbon* **2001**, *39*, 937-950.

45. Celik, B.; Celik, I.; Dolaş, H.; Görçay, H.; Sahin, Y.; Saraç, A. S.; Pekmez, K. *React. Funct. Polym.* **2014**, *83*, 107-112.

46. Ozcan, L.; Sahin, Y.; Türk, H. *Biosens. Bioelectron.* **2008**, *24*, 512-517.

47. Karaca, E.; Pekmez, N. O.; Pekmez, K. *Electrochim. Acta* **2014**, *147*, 545-556.

48. Brillas, E.; Carrasco, J.; Oliver, R.; Estrany, F.; Vilar, J.; Morlans, J. M. *Electrochim. Acta* **2010**, *45*, 4049-4057.

49. Park, J. H.; Ko, J. M.; Park, O. O.; Kim, D. *J. Power Sources* **2002**, *105*, 20-25.

50. Snook, G. A.; Kao, P.; Best, A. A. *J. Power Sources* **2011**, *196*, 1-12.

51. Liu, Y.; Jiang, X.; Li, B.; Zhang, X.; Liu, T.; Yan, X.; Ding, J.; Cai, Q.; Zhang, J. *J. Mater. Chem. A* **2014**, *2*, 4264-4269.

52. Huang, Y.; Li, H.; Wang, Z.; Zhu, M.; Pei, Z.; Xue, Q.; Huang, Y.; Zhi, C. *Nano Energ.* **2016**, *22*, 422-438.

53. Akinwolemiwa, B.; Peng, C.; Chen, G. Z. *J. Electrochem. Soc.* **2015**, *162*, 5054-5059.

54. Dubal, D. P.; Huertas, C.; Holze, R.; Gómez-Romero, P. *Electrochim. Acta* **2016,** *191*, 346-354.

55. Zuo, X.; Zhang, Y.; Si, L.; Zhou, B.; Zhao, B.; Zhu, L.; Jiang, X. *J. Alloy. Compd.* **2016,** *688*, 140-148.

56. Mai, L.; Minhas, A.; Tian, X.; Hercule, K. M.; Zhao, Y.; Lin, X.; Xu, X. *Nat. Commun.* **2013,** *3923*, 1-7.

57. Gan, J. K.; Lim, Y. S.; Pandikumar, A.; Huang, N. M.; Lim, H. N. *RSC Adv.* **2015**, *5*, 12692-12699.

58. Dubal, D. P.; Lee, S. H.; Kim, J. G.; Kim, W. B.; Lokhande, C. D. *J. Mater. Chem.* **2012**, *22*, 3044-3052.

59. Babu, K. F.; Subramanian, S. P. S.; Kulandainathan, M. A. *Carbohyd. Polym.* **2013**, *94*, 487-495.

60. Farma, R.; Deraman, M; Awitdrus; Talib, I. A.; Omar, R.; Manjunatha, J. G.; Ishak, M. M.; Basri, N. H.; Dolah, B. N. M. *Int. J. Electrochem. Sci.* **2013**, *8*, 257-273.

61. Zhang, S.; Peng, C.; Ng, K. C.; Chen, G. Z. *Electrochim. Acta* **2010**, *55*, 7447-7453.

62. Stoller, M. D.; Park, S.; Zhu, Y.; An, J.; Ruoff, R. S. *Nano Lett.*, **2008**, *8*, 3498-3502.

63. Yang, J.; Gunasekaran, S. *Carbon* **2013**, *51*, 36-44.

64. Obeidata, A. M.; Gharaibeh, M. A.; Obaidat, M. *J. Energ. Stor.* **2017**, *13*, 123-128.

65. Ghosh, A.; Lee, Y. H. *ChemSusChem* **2012**, *5*, 480-499.

66. Gamby, J.; Taberna, P. L.; Simon, P.; Fauvarque, J. F.; Chesneau, M. *J. Power Sources* **2001**, *101*, 109-116.

67. Ran, F.; Zhang, X.; Liu, Y.; Shen, K.; Niu, X.; Tan, Y.; Kong, L.; Kang, L.; Xu, C.; Chen, S. *RSC Adv.* **2015**, *5*, 87077-87083.

68. Sarac, A. S.; Sezgin, S.; Ates, M.; Turhan, C. M. *Surf. Coat. Tech.* **2008**, *202*, 3997-4005.

69. Ates, M.; Serin, M. A.; Ekmen, I.; Ertas, Y. N. *Polym. Bull.* **2015**, *72*, 2573-2589.

70. Xu, R.; Guo, F.; Cui, X.; Zhang, L.; Wang, K.; Wei, J. *J. Mater.Chem.* **2015**, *3*, 22353-22360.

71. Biswas, S.; Drzal, L. T. *Chem. Mater.* **2010**, *22*, 5667-5671.

72. Wolfart, F.; Hryniewicz, B. M.; Marchesi, L. F.; Orth, E. S.; Dubal, D. P.; Gómez-Romero, P; Vidotti, M. *Electrochim. Acta* **2017**, *243*, 260-269.

73. Just, P. E.; Chan-Ching, K. I.; Lacaze, P. C. *Tetrahedron* **2002**, *58*, 3467-3472.